Application of contact interactions to Borromean halos

H. Esbensen
Physics Division, Argonne National Laboratory, Argonne, Illinois 60439

G. F. Bertsch and K. Hencken
Institute for Nuclear Theory, University of Washington, Seattle, Washington 98195
(Received 5 May 1997)

^{11}Li and ^{6}He are described as three-body systems using different approaches. We compare our technique, based on a density-dependent, cutoff, contact interaction between the valence neutrons, with a Faddeev approach which is based on realistic interactions. The ground state properties of a weakly bound two-neutron halo are described fairly well once the contact interaction has been adjusted and calibrated to produce a realistic scattering length and effective range. [S0556-2813(97)01212-0]

PACS number(s): 21.30.Fe, 21.45.+v, 21.60.Gx

I. INTRODUCTION

Two-neutron halo (Borromean) nuclei are commonly described as three-body systems consisting of two valence neutrons interacting with each other and with a structureless core. An important theoretical issue is how accurately one must treat the various interactions when truncating the problem to a three-body system. In a previous study of ^{11}Li [1,2] we used a density-dependent, energy-cutoff delta function to simulate the neutron-neutron interaction. An effective interaction of this form has been recognized and used over the past 30 years to study paring phenomena in heavier nuclei (see Sec. II of Ref. [3] for details), and so it is worthwhile to see how reliable this approximation is. By applying it to halo nuclei one may learn how to calibrate it in regions of low density. This is particularly relevant to calculations that try to determine the location of the neutron drip line.

In addition to using a density-dependent δ-function interaction, we also neglected the recoil energy of the core in our earlier work [1,2]. These two approximations together allowed a great simplification in the three-body dynamics, effectively reducing it to a two-body problem. In particular, we were able to calculate the breakup of the nucleus by a dipole field into the three-body continuum without further approximation [2].

In the meantime several three-body Faddeev calculations have been reported [4,5]. They employ realistic two-body interactions between the two valence neutrons and treat recoil of the core exactly. On the other hand, the most sophisticated many-body calculations of light nuclei include in addition also three-body forces which play an important role for obtaining the correct binding energy; see, for example, Ref. [6]. Such three-body forces can be simulated, in an effective theory, by a density-dependent two-body force [7]. In addition, the effective two-body force is also expected to be modified by the nuclear medium of the core.

In order to assess the validity of the two approximations we made in Ref. [1], we repeat in this article the calculation of the ground state, now including the core recoil exactly. This is done by diagonalizing the three-body Hamiltonian in a discretized, truncated space of 0^+ two-particle states. To test the δ-function approximation to the nn interaction, we make comparisons to selected Faddeev calculations. In the comparison some density dependence of the δ-function interaction is justified, in spite of the fact that the Faddeev calculations we compare to do not employ three-body forces. This is discussed in Sec. II B. We shall see that it is possible to adjust the density-dependent nn interaction so that one can reproduce Faddeev calculations. Here it is important to adjust the parameters of the nn interaction so that in free space it gives a realistic scattering length and effective range.

In the comparison to measurements one should also be concerned about the influence of core polarization but we shall not investigate this problem here. A way to study it has been pursued by Nunes *et al.* [8] who extended their three-body model to include explicitly certain core degrees of freedom. They applied their model to ^{12}Be where large effects were expected.

In the next section we define the δ-function nn interaction and discuss how it can be calibrated. The diagonalization of the three-body Hamiltonian is discussed in Sec. III. The results of various calculations of the ground state of ^{11}Li and ^{6}He are presented in Sec. IV, and they are compared to similar Faddeev calculations. Finally we explore in Sec. V the sensitivity of the ^{11}Li ground state to the adopted neutron-core interaction, and Sec. VI contains our conclusions.

II. DENSITY-DEPENDENT δ INTERACTION

The interaction between two neutrons has a strong attraction in the $(T=1, S=0)$ channel and a slight repulsion in the $(T=1, S=1)$ channel. We ignore the latter and approximate the first by a contact interaction. Such an interaction is much too strong to describe pairing phenomena in ordinary nuclei, and so we quench it inside the core by a density-dependent term [1]. The precise form of the quenching is uncertain. Here we adopt for simplicity the form

$$V_{nn}=\delta(\mathbf{r}_1-\mathbf{r}_2)\left(v_0+\frac{v_\rho}{1+\exp[(r_1-R_\rho)/a_\rho]}\right). \quad (2.1)$$

This interaction must be supplemented with a cutoff in the two-particle spectrum, $\epsilon_1+\epsilon_2\leqslant E_{\rm cut}$.

The first term in Eq. (2.1) with v_0 is supposed to simulate the free interaction. It is characterized by two parameters, namely, its strength and the energy cutoff, and we discuss below how they are related to basic features of low-energy scattering. The second term in Eq. (2.1) represents the density-dependent part of the interaction; it is discussed in Sec. II B.

A. Free interaction

The basic quantities that characterize low-energy nn scattering are the scattering length a_{nn} and the effective range r_{nn}. They are parameters in the expansion of $k\cot(\delta)$ in powers of the relative momentum k,

$$k\cot(\delta)\approx -\frac{1}{a_{nn}}+\frac{1}{2}r_{nn}k^2, \tag{2.2}$$

where δ is the s-wave phase shift. The empirical values are $a_{nn}=-18.5\pm 0.5$ fm and $r_{nn}=2.8\pm 0.1$ fm [9].

The three-dimensional δ interaction $V_{nn}=v_0\delta(\mathbf{r}_1-\mathbf{r}_2)$ only has meaning in a truncated space of states. The scattering problem can be exactly solved with the states truncated by a momentum space cutoff, $k\leq k_c$. One obtains the following expression for the phase shifts:

$$k\cot(\delta)=-\frac{2}{\alpha\pi}\left[1+\alpha k_c+\frac{\alpha k}{2}\ln\left(\frac{k_c-k}{k_c+k}\right)\right], \tag{2.3}$$

where

$$\alpha=\frac{v_0}{2\pi^2}\frac{m}{\hbar^2}. \tag{2.4}$$

From Eqs. (2.2) and (2.3) one can derive an expression for the scattering length,

$$a_{nn}=\frac{\pi}{2}\frac{\alpha}{1+\alpha k_c}, \tag{2.5}$$

and for the effective range,

$$r_{nn}=\frac{4}{\pi k_c}. \tag{2.6}$$

The latter is directly related to the cutoff. We shall use an energy cutoff in our Hamiltonian, $E_{\rm cut}=\hbar^2k_c^2/m$. From Eq. (2.6) and the empirical range of 2.8 fm we obtain the cutoff

$$E_{\rm cut}=\frac{\hbar^2}{m}\left(\frac{4}{\pi r_{nn}}\right)^2=8.6\ \text{MeV}. \tag{2.7}$$

We can now characterize the interaction strength v_0 in terms of the scattering length and the cutoff. From Eqs. (2.4) and (2.5) we obtain

$$v_0=2\pi^2\frac{\hbar^2}{m}\alpha=2\pi^2\frac{\hbar^2}{m}\frac{2a_{nn}}{\pi-2k_ca_{nn}}. \tag{2.8}$$

The cutoff (2.7) is rather low and using it for the δ interaction (2.1) would only provide a reasonable fit to the empirical phase shifts at very low energies. This is illustrated in Fig. 1(a), where the dashed curve represents the phase shifts one obtains from the Argonne v_{18} interaction [9]. The results are here presented as $k\cot(\delta)$ as a function of the center-of-mass energy. The Argonne v_{18} result is seen to be very close to a straight line in the depicted energy range. Also shown are the results one obtains from the δ interaction for different energy cutoffs. Here the strength of the interaction has been determined from Eq. (2.8) using the empirical scattering length $a_{nn}=-18.5$ fm. The actual phase shifts are shown in Fig. 1(b).

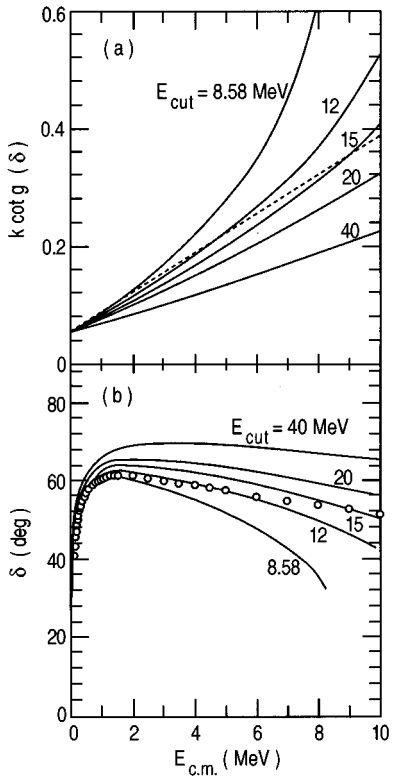

FIG. 1. Calculated nn phase shifts for s-wave scattering obtained from a contact interaction that is based on a scattering length of -18.5 fm and different choices of the energy cutoff $E_{\rm cut}$. In (a) is shown $k\cot(\delta)$ as function of the center-of-mass energy, while (b) shows the actual phase shifts. Also shown are the results obtained from the Argonne v_{18} potential [9] [dashed line in (a) and open circles in (b)].

In our approach to determine the ground state of a two-neutron halo nucleus we discretize the continuum single-particle states by putting them into a radial box. The low cutoff (2.7) does not allow for many states unless we use an extremely large box. Moreover, it is not obvious beforehand exactly which part of the single-particle continuum will dominate the two-neutron ground state. A critical issue is therefore how to make the optimum choice of the parameters of the nn interaction.

B. Density dependence

The radial dependence of the second term in Eq. (2.1) is parametrized as a Fermi function. We used a different parametrization in Ref. [1], in terms of the density, but we do not expect that this will make much difference. In the calculations we discuss later on we have arbitrarily chosen the

diffuseness $a_\rho = 0.67$ fm. This leaves us with two adjustable parameters. In order to reduce this ambiguity let us now try to fix the strength v_ρ.

The formula (2.8) shows a simple relation between the strength and the cutoff in the relative momentum of the two neutrons. However, we will not use a momentum basis to construct our three-particle wave functions but rather a basis of single-particle eigenfunctions of the neutron-core Hamiltonian. We make an energy cutoff in the spectrum corresponding to the free particle momentum cutoff. For a given energy the effective momentum is higher inside the core potential because of the higher kinetic energy of the wave functions there. According to this reasoning, the density-dependent interaction simulates the effect of the changing truncation and can be estimated with the expression

$$v_0 + v_\rho = 2\pi^2 \frac{\hbar^2}{m} \frac{2a_{nn}}{\pi - 2k_c' a_{nn}}, \tag{2.9}$$

where the new momentum cutoff k_c' (expressed in terms of the old one) is

$$k_c' = k_c \sqrt{1 - 2V_{nc}(r=0)/E_c}. \tag{2.10}$$

There are, of course, other phenomena that can invalidate this estimate such as nonlocality and polarization effects, in particular near the surface of the core. We shall, however, use this expression as a guidance to determine v_ρ. Thus we are left with only one unknown parameter, namely, the radius R_ρ, which we adjust so that a known two-neutron separation energy is reproduced.

III. THREE-BODY HAMILTONIAN

The three-body Hamiltonian for two valence neutrons interacting with an inert core has the form

$$H = \frac{p_1^2}{2m} + \frac{p_2^2}{2m} + V_{nc}(1) + V_{nc}(2) + V_{nn} + \frac{(\mathbf{p}_1 + \mathbf{p}_2)^2}{2A_c m}. \tag{3.1}$$

It includes the kinetic energy of each neutron, their interaction V_{nc} with the core, the interaction between the two valence neutrons, and the recoil kinetic energy of the core, which has the mass number A_c. In previous work [1] we ignored the latter term but we include it here in order to investigate its effect.

The single-particle Hamiltonian for a neutron interacting with the core is

$$h_{nc} = \frac{p^2}{2\mu} + V_{nc}(r), \tag{3.2}$$

where $\mu = mA_c/(A_c+1)$ is the reduced mass. The three-body Hamiltonian then takes the form

$$H = h_{nc}(1) + h_{nc}(2) + V_{nn} + \frac{\mathbf{p}_1 \cdot \mathbf{p}_2}{A_c m}. \tag{3.3}$$

The Hamiltonian (3.3) is diagonalized in the space of 0^+ two-neutron states constructed from the eigenstates of the single-particle Hamiltonian h_{nc},

$$\Psi^{(2)}_{nn'\ell j}(\mathbf{r}_1, \mathbf{r}_2) = \sum_m \langle jmj-m|00\rangle \psi_{n\ell jm}(\mathbf{r}_1) \psi_{n'\ell j-m}(\mathbf{r}_2). \tag{3.4}$$

To be more specific, we use as basis the antisymmetric two-particle states that can be constructed from Eq. (3.4), namely,

$$\tilde{\Psi}_{nn'\ell j}(\mathbf{r}_1, \mathbf{r}_2) = \frac{1}{\sqrt{2(1+\delta_{nn'})}} [\Psi^{(2)}_{nn'\ell j}(\mathbf{r}_1, \mathbf{r}_2) + \Psi^{(2)}_{nn'\ell j}(\mathbf{r}_2, \mathbf{r}_1)]. \tag{3.5}$$

Independent two-particle states are restricted by $n' \leq n$. We exclude single-particle states that are occupied by core neutrons. This may introduce some uncertainty because our single-particle Hamiltonian is adjusted to simulate the continuum of the neutron-core system, and it may not be realistic for the Pauli-blocked bound states of the core.

We impose a cutoff in the two-particle spectrum as discussed in Sec. II. We also compare the results we obtain when we include the recoil kinetic energy of the core in the three-body Hamiltonian to the results we obtain without recoil effects, i.e., for $\mathbf{p}_1 \cdot \mathbf{p}_2/(A_c m) = 0$ and $\mu = m$ in Eqs. (3.2) and (3.3). A consistent way to implement the cutoff in the two cases is to include two-particle states with

$$\epsilon_{n\ell j} + \epsilon_{n'\ell j} \leq E_{\rm cut}, \tag{3.6}$$

when the core recoil is ignored, and

$$\epsilon_{n\ell j} + \epsilon_{n'\ell j} \leq \frac{A_c+1}{A_c} E_{\rm cut}, \tag{3.7}$$

when the core recoil is included. Matrix elements of the three-body Hamiltonian H are given in Appendix B of Ref. [1], except for the term $\mathbf{p}_1 \cdot \mathbf{p}_2/(A_c m)$. Its matrix elements may be calculated by Eqs. (A6) and (A7) derived in the Appendix below.

Characteristic distances associated with the ground state include the mean square distance between the two valence neutrons (we call it the squared ''neutron separation''),

$$\langle r^2_{n,n} \rangle = \langle \Psi_{\rm g.s.} | |\mathbf{r}_1 - \mathbf{r}_2|^2 | \Psi_{\rm g.s.} \rangle, \tag{3.8}$$

and the mean square distance of their center of mass with respect to the core (i.e., the mean square ''dineutron-core distance''),

$$\langle r^2_{c,2n} \rangle = \langle \Psi_{\rm g.s.} | |(\mathbf{r}_1 + \mathbf{r}_2)/2|^2 | \Psi_{\rm g.s.} \rangle. \tag{3.9}$$

We shall quote the values we obtain in the different calculations that we have performed. Related combinations of these two quantities, as, for example, the increment in the mean square radius due to the presence of the two valence neutrons,

$$\delta\langle r^2 \rangle = \langle r^2 \rangle_A - \frac{A_c}{A} \langle r^2 \rangle_{A_c} = \frac{1}{A} \left(\frac{2A_c}{A} \langle r^2_{c,2n} \rangle + \frac{1}{2} \langle r^2_{n,n} \rangle \right), \tag{3.10}$$

can then easily be determined.

TABLE I. Ground state properties of ^{11}Li obtained with the shallow neutron-core potential (4.1). All of our calculations employ a radial box of 40 fm; the cutoff in the two-particle spectrum is 15 MeV, except in line 6. Line 7 is the no-recoil limit corresponding to line 5.

Line	Comments	a_{nn} (fm)	S_{2n} (keV)	$\langle r^2_{c,2n}\rangle$ (fm^2)	$\langle r^2_{n,n}\rangle$ (fm^2)	$(s_{1/2})^2$ (%)
1	HHM [10]	−18.5	300	25.0	60.8	98.4
2	Faddeev [11]	−18.5	318	28.1	62.4	95.1
3	$v_\rho=0$	−18.5	569	20.3	49.0	92.1
4	$v_\rho=0$	−9.81	318	26.0	65.3	93.5
5	$v_\rho\neq 0$	−15.0	318	28.3	67.1	92.4
6	$v_\rho\neq 0$, $E_{\rm cut}=25$ MeV	−15.0	318	27.6	62.9	91.1
7	line 5, no recoil	−15.0	318	25.3	67.9	94.4

IV. COMPARISONS TO FADDEEV CALCULATIONS

We apply our three-body model to calculate the ground state of ^{11}Li and ^{6}He and compare the results to similar Faddeev calculations, which are based on realistic *nn* interactions. The comparison will hopefully indicate how reliable our contact interaction (2.1) is.

The empirical knowledge of the structure of ^{11}Li is still quite uncertain, mainly due to uncertainties in the neutron-core interaction. This is discussed and explored in more detail in Sec. V. Here we adopt a shallow neutron-core potential which does not support any bound states. The advantage is that we do not have to worry about effects of Pauli blocking when we compare to the corresponding Faddeev calculation.

The ground state of ^{6}He is under better control. The neutron-core interaction can be calibrated to reproduce the measured low-energy neutron scattering on ^{4}He, and ^{6}He serves therefore as a good test case for three-body models. Finally, we also discuss the results we obtain in the limit where we ignore the recoil of the core nucleus.

A. Shallow single-particle potential

The ground state of ^{11}Li has been studied in several three-body calculations [4,5,10,11] which make use of the shallow neutron-core interaction

$$V_{nc}(r)=-7.8\ \exp[-(r/2.55)^2]\ \ \text{MeV} \qquad (4.1)$$

and a simple Gaussian interaction between the valence neutrons,

$$V_{nn}(r_{12})=-31\ \exp[-(r_{12}/1.8)^2]\ \ \text{MeV}. \qquad (4.2)$$

The *s*-wave phase shifts generated by the latter interaction are in good agreement with the empirical values. We quote the ground state properties that have been obtained from the hyperspherical method [10] in line 1 of Table I. The results have apparently not fully converged since they differ slightly from the results of the most recent Faddeev calculation [11] which are shown in line 2. We shall therefore test our approach against the latter Faddeev calculation.

The results we obtain from the same neutron-core interaction (4.1), and different approximations for the contact interaction between the valence neutrons, are shown in lines 3–5 of Table I. All calculations are based on the same cutoff energy $E_{\rm cut}=15$ MeV and employ single-particle wave functions that are confined to a radial box of 40 fm. The recoil of the core is included in the three-body Hamiltonian, which is diagonalized as described in Sec. III.

In the first calculation (line 3 of Table I) the *nn* interaction (2.1) was determined by a scattering length of $a_{nn}=-18.5$ fm and v_ρ was set to zero. This interaction is clearly too strong; it produces a binding energy of 569 keV. By reducing the *nn* scattering length to -9.81 fm (see line 4) it is possible to reproduce the 318 keV binding energy obtained in the Faddeev calculation. The associated mean square distances are in reasonable but not perfect agreement with the Faddeev calculation.

The *nn* interaction associated with the smaller scattering length is, however, too weak. This is illustrated in Fig. 2 where *nn* phase shifts obtained from different contact interactions are compared to the prediction of the Gaussian inter-

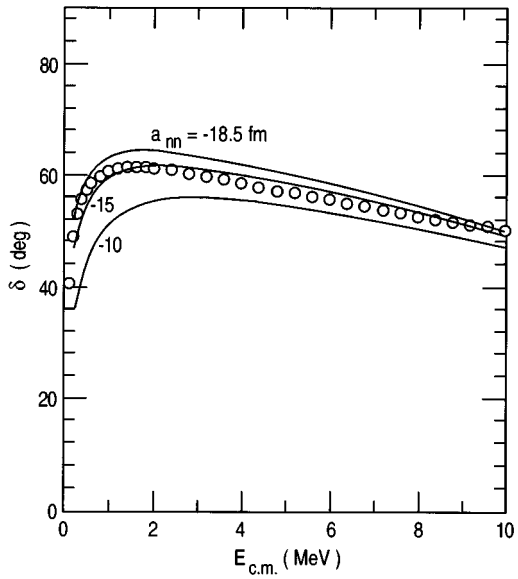

FIG. 2. Calculated *nn* phase shifts for *s*-wave scattering obtained from a contact interaction with an energy cutoff at 15 MeV and different scattering lengths, $a_{nn}=-10$, -15, and -18.5 fm. The open circles are the phase shifts obtained from the Gaussian interaction (4.2).

TABLE II. Results for ground state of ^{6}He. The first three lines have been extracted from Ref. [12]. Our results (lines 4 and 5) were obtained for a nn scattering length of -15 fm and radial box of 30 fm as described in Sec. IV B. Lines 6 and 7 show the corresponding no-recoil limit.

Line	Comments	S_{2n} (keV)	$\langle r^2_{c,2n}\rangle$ (fm^2)	$\langle r^2_{n,n}\rangle$ (fm^2)	$(p_{3/2})^2$ (%)	$S=0$ (%)
1	HH-GPT-WS*	985	11.7	20.3		
2	CSF-SSC-WS*	950	13.0	21.7		88.2
3	CRC-v14-KP*	974	12.3	20.7		
4	$E_{\rm cut}=15$ MeV	975	12.9	29.3	89.2	85.6
5	$E_{\rm cut}=40$ MeV	975	13.2	21.3	83.0	87.0
6	No recoil, $E_{\rm cut}=15$ MeV	975	10.3	29.5	92.0	86.1
7	No recoil, $E_{\rm cut}=40$ MeV	975	10.7	24.3	87.9	87.9

action (4.2). The average ground state kinetic energy for the relative motion of the two neutrons is about 2–3 MeV (cf. line 3 of Table III). It is therefore important to have a realistic nn scattering in this energy range and Fig. 2 shows that a scattering length of -15 fm is a good choice.

In the calculation reported in line 5 of Table I we have therefore adopted the scattering length $a_{nn}=-15$ fm and the same 15 MeV energy cutoff as above. Here we employ the full nn interaction, Eq. (2.1), with the strength $v_\rho=310$ MeV fm^3 determined from Eq. (2.9), and adjust the radius R_ρ to 1.858 fm so that the two-neutron separation energy is reproduced. The resulting mean square neutron separation is seen to be about 7% higher than in the Faddeev calculation. The mean-square dineutron-core distance, on the other hand, is in excellent agreement with the Faddeev calculation.

The small discrepancy in the neutron-neutron distance can be removed by increasing the energy cutoff to 25 MeV, as shown in line 6 of Table I. To reproduce the binding, the radius R_ρ has to increase to 2.096 fm. It is also seen that the distance from the core is insensitive to these adjustments. Finally it is noted that all calculations reported in Table I predict a very large $(s_{1/2})^2$ component in the ground state.

From the above comparison it appears that it is possible to reproduce the Faddeev calculation reasonably well by using a contact interaction that is consistent with low-energy nn scattering. Moreover, the necessary quenching of the nn interaction inside the core is rather modest and consistent with the estimate made in Sec. II B. We shall see that the situation is more problematic when we use a deeper and more realistic neutron-core interaction. A deeper potential requires a larger quenching of the nn interaction inside the core, and the necessary quenching cannot always be predicted. Moreover, for a p-wave-dominated neutron-core Hamiltonian which has a relatively high-lying resonance it is necessary to use a higher-energy cutoff in the two-particle spectrum in order to achieve a realistic ground state. The effective nn interaction will therefore not be consistent with the empirical nn scattering. The situation is not so critical for ^{11}Li, as we shall see in Sec. V, but it is more serious in the case of ^{6}He.

B. Results for ^{6}He

Many three-body calculations have been performed for the ground state of ^{6}He, and we quote three of them in lines 1–3 of Table II. They are based on different methods, namely, the hyperspherical harmonic (HH) expansion, the coordinate space Faddeev (CSF), approach both discussed in Ref. [4], and the coupled reaction channels (CRC) method of Ref. [12]. All of the results quoted here have been extracted from Ref. [12]. The neutron-core potentials have been adjusted slightly in all three cases so that the empirical two-neutron separation energy of 975 keV is roughly reproduced (the asterisk is supposed to indicate that). The three sets of results do not differ much but the Faddeev calculation quoted in line 2 (CSF-SSC-WS*) is probably closest in spirit to our approach and we shall therefore use it for comparisons.

We adjust the neutron-core interaction to reproduce the measured low-energy, neutron-^{4}He phase shifts of Ref. [13]. This can be done by using the parametrization

$$V_{nc}(r)=V_0\left(1-0.44f_{\rm s.o.}r_0^2(\ell\cdot\mathbf{s})\frac{1}{r}\frac{d}{dr}\right)\left[1+\exp\left(\frac{r-R}{a}\right)\right]^{-1}, \tag{4.3}$$

where $R=r_0A_c^{1/3}$, and A_c is the mass number of the core. A good fit to the phase shifts is achieved for the parameter set $a=0.65$ fm, $r_0=1.25$ fm, $V_0=-47.4$ MeV, and $f_{\rm s.o.}=0.93$. The n-^{4}He elastic scattering cross section is dominated by a $p_{3/2}$ resonance and peaks at 0.91 MeV in the center-of-mass system.

The results we obtain by diagonalizing the three-body Hamiltonian (excluding the deeply bound s states) are shown in lines 4 and 5 of Table II, for two different cutoffs in the two-particle energy spectrum. The strength v_0 of the nn interaction (2.1) was determined from a scattering length of -15 fm, as we did in the previous section. It turns out that the nn interaction has to be quenched much more inside the core than predicted by Eqs. (2.9) and (2.10). We do not quite understand the reason for that. We have chosen to set $v_\rho=-v_0$ and adjust the radius R_ρ so that the empirical two-neutron separation energy is reproduced. The required radii are 2.2925 and 2.436 fm, for a 15 and 40 MeV energy cutoff, respectively; they are slightly larger than the radius of the neutron-core potential which is 1.984 fm.

The mean-square dineutron-core distance is insensitive to the energy cutoff and it is in good agreement with the Faddeev calculation. The mean square neutron separation, on the other hand, is quite sensitive to the energy cutoff, and we clearly need a high cutoff, i.e., a small effective range [cf.

TABLE III. Average kinetic and potential energies associated with the relative motion of the core and the center of mass of the two neutrons and with the relative motion of the two neutrons, all in units of MeV. Results are shown for ^{6}He (lines 1 and 2) and for ^{11}Li (line 3). They correspond to the results presented in Tables I and II as indicated in the second column.

Line	See (table,line)	$T_{2n,c}$	$2V_{n,c}$	$E_{2n,c}$	$T_{n,n}$	$V_{n,n}$	$E_{n,n}$	$E_{\rm tot}$
1	^{6}He (II,4)	13.04	−20.74	−7.70	10.68	−3.95	6.73	−0.975
2	^{6}He (II,5)	10.83	−21.23	−10.40	14.17	−4.75	9.42	−0.975
3	^{11}Li (I,5)	1.59	−2.49	−0.90	2.58	−2.00	0.58	−0.318

Eq. (2.6)], in order to reproduce the Faddeev calculation. This is unfortunate because it implies that the contact interaction is no longer consistent with low-energy nn scattering. In the previous case of ^{11}Li, on the other hand, we were able to produce a realistic ground state by employing a realistic contact interaction (although a possibly better fit to the corresponding Faddeev calculation was obtained with a cutoff at 25 MeV).

In order to illustrate in more detail why our approach is not so successful for ^{6}He, we show in Table III the average ground state kinetic and potential energies associated with the relative motion of the core and the center of mass of the two neutrons, and also with the relative motion of the two neutrons. We also show in line 3 the results for ^{11}Li, using the shallow neutron-core interaction. The average kinetic energies are clearly much larger in the case of ^{6}He. There are several reasons for that. First of all, the binding energy is larger than in the case of ^{11}Li, and so the two valence neutrons are much more likely to be inside the core where kinetic energies are large. In addition, the neutron-core potential is much deeper in the case of ^{6}He. Finally, the $p_{3/2}$ resonance of ^{5}He is located at a rather high energy, whereas low-energy s waves dominate in the case of ^{11}Li when we use the shallow neutron-core potential. Consequently, the properties of the calculated ground state of ^{6}He are much more sensitive to the energy cutoff.

C. No-recoil limit

In the no-recoil limit of our model we ignore the last term in the three-body Hamiltonian (3.1). If we just do that, we obtain a two-neutron separation energy that is much too large, and so we need to make additional corrections. The recoil term is directly related to the relative motion of the dineutron and the core, whereas the relative motion of the two neutrons is not directly affected by the recoil term. The simplest way to fix the problem associated with the excessive binding is to reduce the strength of the neutron-core interaction. We have chosen to reduce the neutron-core interaction by the factor $A_c/(A_c+1)$. The single-particle wave functions we obtain in the no-recoil limit (i.e., for $\mu=m$) are then identical to the eigenfunction of the Hamiltonian (3.2), not for a fixed energy, but for a fixed wave number.

The results we obtain for ^{11}Li and ^{6}He by adopting this definition of the no-recoil limit are given in line 7 of Table I and lines 6 and 7 in Table II, respectively. In both cases we have slightly adjusted the radius parameter R_ρ in the contact interaction (2.1) in order to reproduce the binding energies. The mean square neutron separations are seen to be slightly larger in the no-recoil limit. The main difference from the results which include the recoil is that the mean-square dineutron-core distance is significantly smaller; the reduction is close to the factor $A_c/(A_c+1)$. Since the total dipole strength associated with the halo is proportional to this mean square distance, one would clearly underestimate the dipole strength in the no-recoil limit.

V. REALISTIC CALCULATIONS FOR ^{11}Li

We shall now try to incorporate and explore the consequences of the current empirical knowledge about the ground state of ^{11}Li. First of all, we always adjust the quenching of the nn contact interaction (2.1) inside the core so that the measured two-neutron separation energy [14] of 295 ± 35 keV is reproduced. Next we adjust the neutron-core interaction so that it produces a $p_{1/2}$ resonance near 540 keV, as suggested by measurements of the ^{11}B(^{7}Li,^{8}B)^{10}Li reaction [15]. The result, as we shall see, is a ground state with 85–90 % of the valence neutrons in $(p_{1/2})^2$ configurations.

Finally, we explore the influence of a stronger s-wave scattering in the neutron-core system. Several experiments seem to indicate that the ground state of the ^{11}Li halo has a large s-wave component [15–17]. The measurement of the β decay of ^{11}Li to the first $1/2^-$ excited state in ^{11}Be [17], for example, has been interpreted as evidence for a smaller $(p_{1/2})^2$ component, of 51 ± 6 %.

A. Role of p waves in ^{11}Li

The neutron-core interaction is again parametrized as in Eq. (4.3) with $a=0.67$ fm and $r_0=1.27$ fm. We adjust the depth, $V_0=-35.366$ MeV, and the spin-orbit strength, $f_{\rm s.o.}=1.006$, so that the neutron-core elastic scattering cross section has a maximum near 540 keV, and so that the bound $p_{3/2}$ state appears at -2.033 MeV as in ^{8}Li. This bound state, and also the deeply bound s state, will be blocked when we diagonalize the three-body Hamiltonian.

Ideally, the neutron-core interaction should be tested against the elastic scattering of neutrons on a ^{9}Li target but such data do not exist. Our prediction is shown in Fig. 3 and we compare it to the ^{11}B(^{7}Li,^{8}B)^{10}Li reaction data of Ref. [15], although an interpretation of a comparison may be doubtful. The measured peak around 540 keV is well reproduced but the data suggest an additional, possibly s-wave strength, close to threshold. This will be simulated in the next subsection.

The ground state properties we obtain by adopting this neutron-core interaction in the three-body calculation are

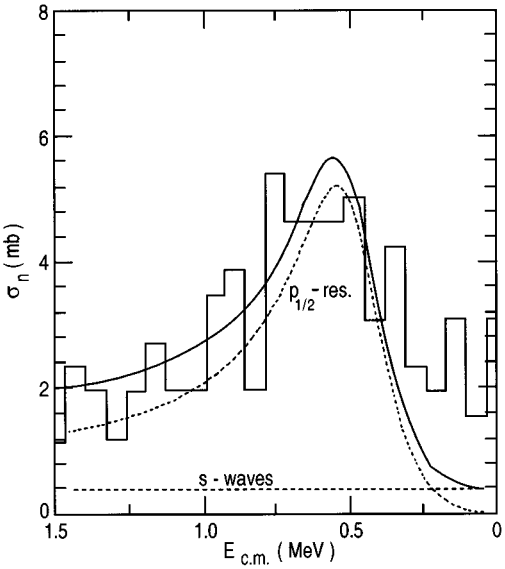

FIG. 3. The calculated elastic scattering cross section of neutrons on ^{9}Li discussed in the text. The solid curve is the total. The two dashed curves are the separate contributions from s waves and from the $p_{1/2}$ resonance, respectively. The histogram shows the ^{11}B(^{7}Li,^{8}B)^{10}Li reaction data from Ref. [15].

given in line 1 of Table IV. The nn interaction is here the same outside the core as used in line 5 of Table I, namely, a contact interaction generated by a scattering length of -15 fm and an energy cutoff at 15 MeV. It is also necessary to quench the interaction (2.1) inside the core. The radius R_ρ was set equal to the radius of the neutron-core potential, and the strength, v_ρ=640.5 MeV fm^3, was adjusted so that the empirical binding energy was reproduced. It is reassuring that this strength does not differ much from the estimate made in Eqs. (2.9) and (2.10) which predicts v_ρ=629 MeV fm^3.

The results we obtain if we instead choose $E_{\rm cut}$=30 MeV are shown in line 2 of Table IV. The parameters of the three-body Hamiltonian are the same as for the 15 MeV cutoff, except the strength v_ρ which has now been adjusted to 561 MeV fm^3. The mean-square dineutron-core distance does not change much by this adjustment but the neutron separation becomes smaller. This trend is similar to what we saw previously, namely, that a higher cutoff implies a smaller effective range and therefore a smaller separation between the two valence neutrons.

The ground state is in both cases dominated by $(p_{1/2})^2$ configurations, and the $S=0$ component is only 43%. Without spin-orbit splitting, the latter component would be 100% as it is for the shallow neutron-core potential discussed in Sec. IV A. The characteristic mean square distances of the two-neutron halo are seen to be much smaller than those obtained for the shallow neutron-core potential quoted in Table I. To increase their values we clearly need a larger s-wave component.

Unfortunately, we cannot in this particular case make comparisons to a Faddeev calculation which reproduces the empirical binding energy and, at the same time, is based on the same neutron-core potential. We quote an example (model Q9 of Ref. [4]) in line 3, which gives a realistic binding energy of 296 keV, but the p-wave resonance of the adopted neutron-core Hamiltonian is located at 200 keV, somewhat lower than our choice. The resulting mean square distances are both slightly larger than both of our results. In spite of the uncertainty in the comparison, it appears that our model is able to produce a ground state that does not differ much from the Faddeev calculation. Moreover, this can be done with a contact interaction that is in reasonable agreement with the empirical nn scattering, namely, with $E_{\rm cut}$ =15 MeV and $a_{nn}=-15$ fm.

B. Role of s waves in ^{11}Li

In order to increase the s-wave component of the ground state, we use a different well depth in Eq. (4.3) for even-parity single-particle states and increase it to -47.5 MeV. This produces an s-wave, neutron-core scattering length of $a_{nc}=-5.6$ fm. For the odd-parity states we use the same well depth as earlier so that the $p_{1/2}$ resonance is unchanged. We do not show the total elastic scattering cross section but mention that it is now consistent with the reaction data [15] shown in Fig. 3, in particular at low energies.

Using this modified neutron-core interaction in our three-body calculation we obtain the results shown in line 5 of Table IV. The contact interaction is again based on the nn

TABLE IV. Ground state properties of ^{11}Li for a binding energy of 295 keV. The radial box size was 40 fm and the adopted nn scattering length was -15 fm. Lines 1 and 2 were based on a neutron-core interaction that produces a $p_{1/2}$ resonance at 540 keV, and an s-wave scattering length of $a_{nc}=+1.7$ fm. Line 5 was based on a stronger interaction in even-parity states, producing an s-wave scattering length of $a_{nc}=-5.6$ fm. A particular set of Faddeev results [4], based on a $p_{1/2}$ resonance at 200 keV and a realistic nn interaction, is shown in line 3 for comparison. Line 4 is the results we obtained previously [1] in the no-recoil limit, with a two-neutron binding energy of 200 keV and a neutron-core $p_{1/2}$ resonance at 800 keV.

Line	Comments	$\langle r^2_{c,2n}\rangle$ (fm^2)	$\langle r^2_{n,n}\rangle$ (fm^2)	$(s_{1/2})^2$ (%)	$(p_{1/2})^2$ (%)
1	$a_{nc}=1.7$ fm, $E_{\rm cut}=15$ MeV	18.7	42.8	4.5	89.1
2	$a_{nc}=1.7$ fm, $E_{\rm cut}=30$ MeV	18.3	37.6	4.6	85.3
3	Q9 of Ref. [4]	21.2	44.9		
4	Ref. [1], no recoil	24.3	39.0	6.1	76.9
5	$a_{nc}=-5.6$ fm, $E_{\rm cut}=15$ MeV	26.2	45.9	23.1	61.0

scattering length of -15 fm and an energy cutoff of 15 MeV. To reproduce the empirical binding energy we have to use a stronger quenching and set $v_\rho = -v_0 = 1160$ MeV fm^3 and adjust R_ρ to 3.045 fm, which is larger that the radius $R = 2.642$ fm of the neutron-core potential. Compared to the result shown in line 1 of Table IV, the s-wave component of the ground state has now increased from 4.5% to 23%, and the p-wave component is reduced from 89% to 61%. The mean-square dineutron-core distance has also increased substantially and it is now close to but slightly larger than the value we obtained in our old model of ^{11}Li [1] which is quoted in line 4 of Table IV.

It is appropriate at this point to make a few comments on the ground state and the dipole response that we obtained in the old model [1,2]. It was based on the no-recoil limit and gave a two-neutron separation energy of 200 keV. This was achieved by placing the neutron-core $p_{1/2}$ resonance at 800 keV and using a nn contact interaction that had an infinite scattering length and a cutoff energy of 40 MeV. The model gave a good description of measured breakup cross sections [18] and also of measured momentum distributions for Coulomb dissociation [19]. There were some discrepancies in the momentum distribution of ^{9}Li fragments with respect to the center of mass of the two neutrons and a similar discrepancy in the decay energy spectrum, where the data [20,21] showed a peak located at a higher excitation energy than predicted by the model [19]. The comparison [18] with measured cross sections indicates, however, that the total dipole strength of the model is realistic.

The fact that the new model, which includes the core recoil and contains a substantial amount of s waves in the ground state (line 5 of Table IV), predicts a slightly larger mean square distance between the core and the two neutrons than obtained in the old model, and therefore also a slightly larger total dipole strength, looks promising for a successful outcome. Moreover, the effects of a larger binding energy, and also of a weaker nn interaction associated with a realistic nn scattering length that we have in the new model, may put the peak of the dipole response at a higher excitation energy as required by the Coulomb dissociation data [20,21]. Unfortunately, the computational technique we used for the dipole response of the three-body system is valid only in the no-recoil limit [2]. We would therefore have to develop a new way to calculate the dipole response which includes recoil effects.

VI. CONCLUSION

Our goal is to construct reliable models of halo nucleus wave functions, making use of the known free nn interaction and whatever information about the neutron-core interaction is available. It is too much to ask such a model to predict binding energies to the required accuracy, and we adjust the quenching of the nn interaction inside the core to fit the binding energy. The properties of the ground state wave function that we have examined are the average separation of the two neutrons, the distance of the neutron pair from the core, and the single-particle angular momentum probabilities. The dipole strength function is sensitive to the distance from the core and the momentum distribution of the remaining neutron following a one-neutron-stripping reaction is sensitive to its angular momentum. The average separation of the two neutrons is important in the (^{11}B, ^{11}Li) pion double-charge-exchange reaction, in the β-delayed deuteron emission from ^{11}Li, and it may also affect the cross sections for two-neutron stripping as compared to one-neutron stripping.

We have tested our technique by comparing with the Faddeev method. The comparison can best be done for a shallow neutron-core interaction that does not support any bound states, because of the different approaches to dealing with the Pauli principle with respect to core nucleons. We found that the necessary density dependence to fit the binding energy was rather mild, and that the neutron separation and the dineutron-core distance agree rather well with the Faddeev results. The s-orbital probabilities are all over 90% in these models. We also found that the no-recoil approximation works quite well. In our no-recoil approximation, the squared dineutron-core distance is reduced by a factor $A_c/(A_c+1)$ while the neutron separation remains the same.

We next consider models of ^{6}He with a realistic neutron-core interaction. The average kinetic energy of the neutron pair is much larger in this case, and the required density dependence of the nn interaction is much stronger. The model no longer agrees with the Faddeev calculation on the separation between the two neutrons, unless the effective range of the interaction is considerably reduced. However, the dineutron-core distance and also the $S=0$ probability are insensitive to the effective range and agree with the Faddeev results.

The neutron-core potential for ^{11}Li is subject to doubt. The most straightforward model is a Woods-Saxon potential fit to the observed $p_{1/2}$ resonance at 540 keV. This leads to a large $(p_{1/2})^2$ component in the ground state. Several ^{11}Li experiments [15–17] suggest a smaller $(p_{1/2})^2$ component or, conversely, a larger $(s_{1/2})^2$ component. We accommodate for that by using a different well depth for even-parity single-particle states, and adjust it to produce an s-wave scattering length of -5.6 fm. The new halo ground state has now a significant $(s_{1/2})^2$ component of 23%. This enhances the dineutron-core distance and therefore also the total dipole strength of the halo, to a level that is needed to explain measured Coulomb dissociation cross sections. It remains to be seen if this ground state can also explain other reaction data, or if we have to enhance the $(s_{1/2})^2$ component even further. We intend to focus on the decay energy spectrum of a single neutron and the ^{9}Li fragment produced in single-neutron stripping reactions, since such data have now become available [22].

ACKNOWLEDGMENTS

This work was supported in part by the U.S. Department of Energy, Nuclear Physics Division, under Contract Nos. W-31-109-ENG-38 and DE-FG-06-90ER-40561. One of us (K.H.) acknowledges support by the Swiss National Science Foundation (SNF), the ''Deutsche Forschungsgemeinschaft'' (DFG), and the ''Freiwillige Akademische Gesellschaft'' (FAG) of the University of Basel.

APPENDIX: RECOIL TERM

In order to diagonalize the three-body Hamiltonian we need the matrix elements between all 0^+ two-particle states. Most of the terms are given in Appendix B of Ref. [1]; the only term left is the matrix elements of $\nabla_1 \cdot \nabla_2$ which we derive here. The two-particle wave functions with total angular momentum 0^+ have the form [cf. Eq. (A4) of Ref. [1]]

$$\Psi_{nn'\ell j}(\mathbf{r}_1,\mathbf{r}_2) = \phi_{n\ell j}(r_1)\phi_{n'\ell j}(r_2)\frac{1}{\sqrt{4\pi}} \times \sum_{m_1 m_2 m_\ell} C^{\ell j}_{m_1 m_2} Y_{\ell m_\ell}(\theta) \times \chi^{(1)}_{m_1}\chi^{(2)}_{m_2}\delta_{m_\ell,-(m_1+m_2)}, \quad \text{(A1)}$$

where m_1 and m_2 are the spin projections of the two particles ($m_1 = \pm 1/2, m_2 = \pm 1/2$), θ is the angle between r_1 and r_2, and the C coefficients are given in Eqs. (A6a) and (A6b) of Ref. [1].

To calculate matrix elements of $\nabla_1 \cdot \nabla_2$ between any two two-particle states of the form (A1) it is convenient to express ∇ in terms of the commutator (see, for example, p. 433 of Ref. [23]),

$$\nabla = \frac{1}{2}[\nabla^2, \mathbf{r}] = \frac{1}{2}[\nabla^2, r\hat{r}], \quad \text{(A2)}$$

where $\hat{r}$ is the unit vector in the direction of $\mathbf{r}$. Inserting

$$\nabla^2 = \frac{d^2}{dr^2} + \frac{2}{r}\frac{d}{dr} - \frac{\ell^2}{r^2}, \quad \text{(A3)}$$

where ℓ is the angular momentum operator, we obtain

$$\nabla = \hat{r}\frac{1}{2}\left[\frac{d^2}{dr^2} + \frac{2}{r}\frac{d}{dr}, r\right] - \frac{1}{2r}[\ell^2, \hat{r}] = \hat{r}\left(\frac{d}{dr} + \frac{1}{r}\right) - \frac{1}{2r}[\ell^2, \hat{r}]. \quad \text{(A4)}$$

This form separates nicely the radial and angular dependence and makes it fairly easy to calculate the matrix elements.

The radial single-particle matrix elements associated with Eq. (A4) have the form

$$R(n_1\ell_1 j_1; n_2\ell_2 j_2) = \int dr r^2 \phi_{n_1\ell_1 j_1}(r) \times \left(\frac{d}{dr} + \frac{1}{r} - \frac{1}{2r}[\ell_1(\ell_1+1) - \ell_2(\ell_2+1)]\right)\phi_{n_2\ell_2 j_2}(r). \quad \text{(A5)}$$

Here we have replaced the operator ℓ^2 by its eigenvalue in the two single-particle states. All that is left from Eq. (A4) is the orientation vector $\hat{r}$.

We can now calculate the desired matrix element of $\nabla_1 \cdot \nabla_2$. Since it is diagonal in the spin quantum numbers, we obtain,

$$\langle \Psi_{n_1 n_1' \ell_1 j_1} | \nabla_1 \cdot \nabla_2 | \Psi_{n_2 n_2' \ell_2 j_2} \rangle = R(n_1\ell_1 j_1; n_2\ell_2 j_2) R(n_1'\ell_1 j_1; n_2'\ell_2 j_2) \times \sum_{m_1 m_2 m_\ell} \delta_{m_\ell,-(m_1+m_2)} C^{\ell_1 j_1}_{m_1 m_2} C^{\ell_2 j_2}_{m_1 m_2} \times \langle Y_{\ell_1 m_\ell} | \hat{r}_1 \cdot \hat{r}_2 | Y_{\ell_2 m_\ell} \rangle. \quad \text{(A6)}$$

The angular dependence is contained in the last matrix element. Here $\hat{r}_1 \cdot \hat{r}_2 = \cos(\theta)$, where θ is the relative angle between $\mathbf{r}_2$ and $\mathbf{r}_1$. The two-particle wave functions (A1) depend on the same angle, and so we obtain

$$\langle Y_{\ell_1 m_\ell} | \hat{r}_1 \cdot \hat{r}_2 | Y_{\ell_2, m_\ell} \rangle = \langle Y_{\ell_1 m_\ell} | \cos(\theta) | Y_{\ell_2, m_\ell} \rangle = \sqrt{\frac{(\ell_> + m_\ell)(\ell_> - m_\ell)}{(2\ell_>+1)(2\ell_>-1)}}, \quad \text{(A7)}$$

where $\ell_> = \max\{\ell_1, \ell_2\}$ and $\ell_2 = \ell_1 \pm 1$.

[1] G. F. Bertsch and H. Esbensen, Ann. Phys. (N.Y.) **209**, 327 (1991).
[2] H. Esbensen and G. F. Bertsch, Nucl. Phys. **A542**, 310 (1992).
[3] J. Dobaczewski *et al.*, Phys. Rev. C **53**, 2809 (1996).
[4] M. V. Zhukov *et al.*, Phys. Rep. **231**, 151 (1993).
[5] D. V. Federov, E. Garrido, and A. S. Jensen, Phys. Rev. C **51**, 3052 (1995).
[6] B. S. Pudliner, V. R. Pandharipande, J. Carlson, and R. B. Wiringa, Phys. Rev. Lett. **74**, 4396 (1995).
[7] D. Zawischa, U. Regge, and R. Stapel, Phys. Lett. B **185**, 299 (1987).
[8] F. M. Nunes, J. A. Christley, I. J. Thompson, R. C. Johnson, and V. D. Efros, Nucl. Phys. **A609**, 43 (1996).
[9] R. B. Wiringa, V. G. J. Stoks, and R. Schiavilla, Phys. Rev. C **51**, 38 (1995).
[10] M. V. Zhukov *et al.*, Phys. Lett. B **265**, 19 (1991).
[11] Ian Thompson (private communication).
[12] S. Funada, H. Kameyama, and Y. Sakuragi, Nucl. Phys. **A575**, 93 (1994).
[13] R. A. Arndt, D. D. Long, and L. D. Roper, Nucl. Phys. **A209**, 429 (1973).
[14] B. M. Young *et al.*, Phys. Rev. Lett. **71**, 4124 (1993).
[15] B. M. Young *et al.*, Phys. Rev. C **49**, 279 (1994).
[16] R. A. Kryger *et al.*, Phys. Rev. C **47**, R2439 (1993).
[17] N. Aoi *et al.*, Nucl. Phys. **A616**, 181 (1997).
[18] H. Esbensen and G. F. Bertsch, Phys. Rev. C **46**, 1552 (1992).
[19] H. Esbensen, G. F. Bertsch, and K. Ieki, Phys. Rev. C **48**, 326 (1993).
[20] D. Sackett *et al.*, Phys. Rev. C **48**, 118 (1993).
[21] S. Shimoura *et al.*, Phys. Lett. B **348**, 29 (1995).
[22] M. Zinser *et al.*, Nucl. Phys. **A619**, 151 (1997).
[23] R. D. Lawson, *Theory of the Nuclear Shell Model* (Clarendon Press, Oxford, 1980).